Climate Data Record (CDR) Program

Technical Note for IASI/CrIS Data Extension for Outgoing Longwave Radiation (OLR) – Daily

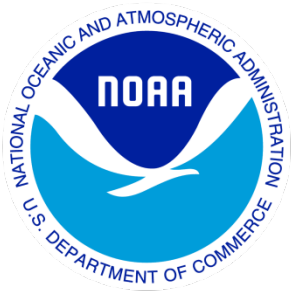

CDR Program Document Number: CDRP-RPT-1442
Configuration Item Number: 01B-21
Revision 0 / Nov 13, 2023
DSR Number: DSR-1840

REVISION HISTORY

Rev.	Author	DSR No.	Description	Date
0	Hai-Tien Lee Univ. of Maryland	DSR-1840	Technical Note for IASI/CrIS data extension for OLR-Daily 2007 - current	11/01/2023

TABLE of CONTENTS

INTRODUCTION 6
1.1 Purpose 6
1.2 Referencing this Document 6
1.3 Products Relevant to this Document 6

IASI AND CRIS OLR RETRIEVALS 8
2.1 IASI and CrIS OLR Algorithms 8
2.2 Data availability 11

INTER-SATELLITE CALIBRATION 12
3.1 Calibrate M02 IASI against M02 HIRS 12
3.2 Calibrate remaining IASI/CrIS against M02 IASI 13

CHANGES FROM DAILY OLR CDR V1.2 TO V1.3 14
4.1 Evaluation with CERES SYN1deg data 14
4.2 Evaluation with CERES EBAF data 18

REFERENCES 23

ACKNOWLEDGMENT 24

LIST of FIGURES

Fig. 1 Correlation between spectral fluxes and radiances at different local zenith angles. 9

Fig. 2 Selections of predicting radiances (y-axis) for the estimation of spectral fluxes (x-axis) at each 10 cm-1 wavenumber band, with IASI radiance observations in 650-2500 cm-1 range. There are three selected predicting radiances wavenumbers at each spectral band, represented by colors red, blue and green. 10

Fig. 3 RMS regression errors for the total OLR estimation, as a function of the observing local zenith angle, range from 0.13 - 0.47 Wm-2, and are dominated by flux estimation errors from the “FIR” spectral domain. 10

Fig. 4 Equator crossing times for the ascending orbit of the NOAA POES TIROS-N, Metop and JPSS-series satellites. 11

Fig. 5 Monthly mean nodal maps of OLR differences between M02-IASI and M02-HIRS for March 2009 before (top row) and after (bottom row) the application of the zonal intersatellite calibration adjustment. 13

Fig. 6 Mean OLR differences for (a) v1.2 and (b) v1.3 Daily OLR CDR, relative to CERES SYN1deg-Daily Ed4.1 OLR product, over 2000.03-2022.12 period. 14

Fig. 7 Standard Deviation of OLR differences for (a) v1.2 and (b) v1.3 Daily OLR CDR, relative to CERES SYN1deg-Daily Ed4.1 OLR product, over 2000.03-2022.12 period. 15

Fig. 8 Global mean OLR differences for (a) v1.2 and (b) v1.3 Daily OLR CDR, relative to CERES SYN1deg-Daily Ed4.1 OLR product, over 2000.03-2022.12 period. 15

Fig. 9 Tropical 20S-20N mean OLR differences for (a) v1.2 and (b) v1.3 Daily OLR CDR, relative to CERES SYN1deg-Daily Ed4.1 OLR product, over 2000.03-2022.12 period. 15

Fig. 10 Differences of global OLR anomalies for (a) v1.2 and (b) v1.3 Daily OLR CDR, relative to CERES SYN1deg-Daily Ed4.1 OLR product, over 2000.03-2022.12 period. 16

Fig. 11 Differences of tropical OLR anomalies for (a) v1.2 and (b) v1.3 Daily OLR CDR, relative to CERES SYN1deg-Daily Ed4.1 OLR product, over 2000.03-2022.12 period. 16

Fig. 12 Global mean OLR differences for v1.2 and v1.3 Daily OLR CDR, relative to CERES SYN1deg-Daily Ed4.1 OLR product. It shows improved stability (see green curve) and reduced random errors (red curve) in v1.3 Daily OLR CDR, particularly after 2014. 17

Fig. 13 Comparison of the standard deviation of zonal OLR differences v1.2 (blue) and v1.3 (orange) Daily OLR CDR, relative to CERES SYN1deg-Daily Ed4.1 OLR product. It shows significant reduction of the uncertainties across the latitudinal zones. 17

Fig. 14 Mean OLR differences for (a) v1.2 and (b) v1.3 Daily OLR CDR, relative to CERES EBAF Ed4.2 OLR product, over 2000.03-2022.12 period. 19

Fig. 15 Standard Deviation of OLR differences for (a) v1.2 and (b) v1.3 Daily OLR CDR, relative to CERES EBAF Ed4.2 OLR product, over 2000.03-2022.12 period. 19

Fig. 16 Global mean OLR differences for (a) v1.2 and (b) v1.3 Daily OLR CDR, relative to CERES EBAF Ed4.2 OLR product, over 2000.03-2022.12 period. 19

Fig. 17 Differences of global OLR anomalies for (a) v1.2 and (b) v1.3 Daily OLR CDR, relative to CERES EBAF Ed4.2 OLR product, over 2000.03-2022.12 period. 20

Fig. 18 Differences of tropical OLR anomalies for (a) v1.2 and (b) v1.3 Daily OLR CDR, relative to CERES EBAF Ed4.2 OLR product, over 2000.03-2022.12 period. 20

Fig. 19 Differences of global OLR anomalies for (a) v1.2 and (b) v1.3 Daily OLR CDR, relative to CERES SYN1deg-Daily Ed4.1 OLR product, over 2000.03-2022.12 period. 21

Fig. 20 Differences of tropical OLR anomalies for (a) v1.2 and (b) v1.3 Daily OLR CDR, relative to CERES SYN1deg-Daily Ed4.1 OLR product, over 2000.03-2022.12 period. 21

LIST of TABLES

Table 1 Version tracking for the DAILY OLR CDR product releases. 6

Table 2 Data availability of IASI and CrIS observations. 11

Table 3 Summary statistics for the evaluation of Daily OLR CDR v1.2 and v1.3, in reference to CERES SYN1deg-daily Ed4.1 product, over 2000.03-2022.12 period. 18

Table 4 Summary statistics for the evaluation of Daily OLR CDR v1.2 and v1.3, in reference to CERES EBAF Ed4.2 product, over 2000.03-2022.12 period. 22

Introduction

1.1 Purpose

The objective of this document is to furnish details about the updated Daily Outgoing Longwave Radiation (OLR) Climate Data Record (CDR) dataset, version v01r02, spanning from 2007 to the present, featuring an extension incorporating IASI/CrIS data.

For the current operational v01r02 Daily OLR CDR, refer C-ATBD by Lee (2014) and publication of Schreck et al. (2018)

This release serves as an interim measure to guarantee the accessibility and uninterrupted continuity of the OLR CDR dataset, given the imminent possibility of decommissioning of HIRS instruments. In light of its provisional nature to address the present circumstances, the version number and file names remain unchanged, with modifications limited to metadata updates.

The internal designation for the extended IASI/CrIS data from 2007 to the present will be referred to as "v1.3" henceforth, whereas the previous v01r02 operational product will be labeled as "v1.2" to ensure clear distinction.

Previously the OLR CDR relied primarily on HIRS OLR retrievals. Recent years we have discovered artifacts in trends and uncertainties due to deteriorating HIRS instruments and the unfavorable orbital drift towards evening hours. The inclusion of IASI/CrIS OLR retrievals not only enhances the accuracy of OLR retrievals but also complements diurnal sampling. This effectively mitigates trend artifacts and significantly improves overall accuracy.

The forthcoming significant upgrade, set for release in June 2025 as Daily OLR CDR v02r00, will encompass a comprehensive reprocessing of the entire Daily OLR CDR dataset dating back to 1979. This initiative is aimed at effectively addressing and rectifying the issues that have been identified and persisted throughout the years.

1.2 Referencing this Document

This document should be referenced as follows:

Technical Note for IASI/CrIS Data Extension for OLR-Daily CDR.

1.3 Products Relevant to this Document

Table 1 describes the versions of the Daily OLR CDR product releases with their corresponding software package and the CATBD versions.

Table 1 Version tracking for the DAILY OLR CDR product releases.

Product Version	Software Version	CATBD Revision	Release Date	Remarks

v01r02	v01r02	v1	2014-06-10	Initial Release
v01r02	v01r02	Technical Note for IASI/CrIS Data Extension 2007-present for Daily OLR CDR	2023-11-01	Intermediate release. Version unchanged. See Technical note.
v02r00	v02r00	v2	2025-06-30	Major update

IASI and CrIS OLR Retrievals

2.1 IASI and CrIS OLR Algorithms

The hyperspectral OLR estimation principles and IASI OLR retrieval algorithm are explained here.

The total outgoing longwave radiative flux density, OLR, is the integral of the spectral fluxes over the thermal radiation spectrum,

$$\mathrm{OLR} = \int \mathrm{F}_\nu \mathrm{d}\nu \quad (1)$$

The spectral flux F_ν $at\ frequency\ \nu$ is the integral of the normal specific radiances at the top of the atmosphere z_t, over the hemispheric dome related to the local zenith angle θ and azimuthal angle ϕ,

$$\mathrm{F}_\nu = \int_0^{2\pi} \int_0^{\pi/2} \mathrm{I}_\nu(\mathrm{z_t};\ \theta, \phi) \cos\theta \sin\theta \, \mathrm{d}\theta \, \mathrm{d}\phi \quad (2)$$

Frequency-dependent Spectral Angular Models (SAM), can be constructed to approximate the spectral flux integral, for a radiance observation at local zenith angle θ, such that,

$$\mathrm{F}_\nu \cong \mathrm{SAM}_\nu(\mathrm{I}_\nu(\mathrm{z_t};\ \theta)) \quad (3)$$

There are two principles that make the spectral flux estimation possible with the spectral angular models:

1. ***Inter-Frequency Correlations*** *- Radiances at one frequency are strongly correlate with radiances at another with similar absorption features.*
2. ***Intra-Frequency/Angle Correlations*** *- Using "absorption strength" as surrogate to "optical path length", spectral flux integration can be estimated with radiances at selected angles (as in Gaussian quadrature)*

Previous works can be found in Lee, Ellingson & Gruber (2010); Turner, Lee & Tett (2015).

The IASI OLR algorithm is a 3-predictor multiple linear regression model in quadratic forms, whereas the predictors are natural log of IASI radiances aggregated to 10 cm^{-1} intervals in 650-2500 cm^{-1} range. Note that the IASI radiance observations over 2500-2760 cm^{-1} are not used due to possible solar contamination.

$$\begin{aligned} log(F_\nu) = {} & a_0(\nu,\theta) + a_1(\nu,\theta)\, x_1(\nu,\theta) + a_2(\nu,\theta)\, x_2(\nu,\theta) + \\ & a_3(\nu,\theta)\, x_3(\nu,\theta) + a_4(\nu,\theta)\, \mathrm{x}_1^2(\nu,\theta) + \\ & a_5(\nu,\theta)\, \mathrm{x}_2^2(\nu,\theta) + a_6(\nu,\theta)\, \mathrm{x}_3^2(\nu,\theta) \end{aligned} \quad (4)$$

where,

$$\mathrm{x}_\nu = \log(\mathrm{I}_\nu(\theta)) \quad (5)$$

with the frequency and zenith angle-dependent regression coefficients a's.

Figure 1 shows the correlations between the spectral flux and radiance at different zenith angles. The strongest correlations can be seen near 53° and this is related to the diffusivity approximation. The spectral locations with strong absorption features tend to produce weaker correlations for zenith angles outside vicinity of 53°, and this is where the Intra-frequency/angle correlations become useful for the spectral flux estimation.

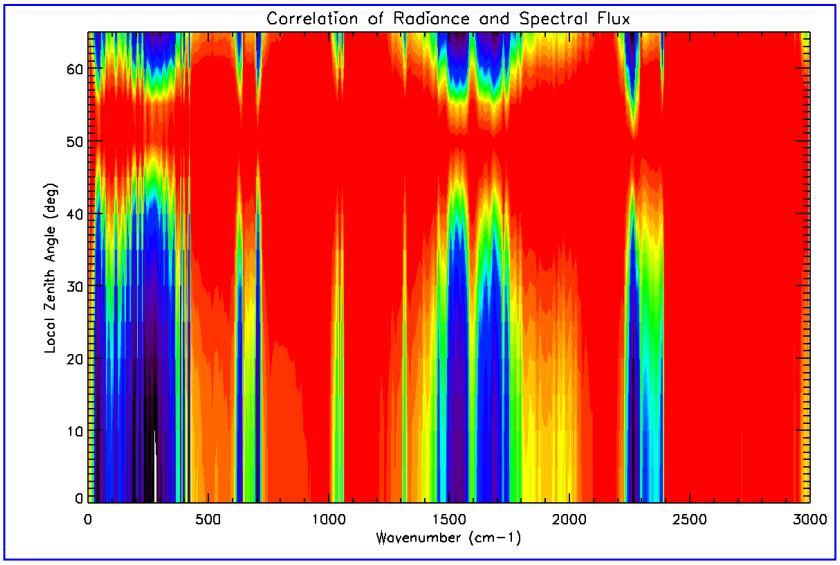

Fig. 1 Correlation between spectral fluxes and radiances at different local zenith angles.

Figure 2 shows the selection of the predicting radiances for the estimation of spectral fluxes at each 10 cm^{-1} wavenumber band. The estimate of the IASI OLR estimation errors are shown in **Figure 3**, where the rms total estimation errors range from 0.13 - 0.47 Wm^{-2}. The far infrared (FIR) spectral domain, 0-650 cm^{-1} contributed the most of the errors, due that the FIR spectrum are not directly observed and the spectral fluxes are not well correlated to radiance observations at most of the angles.

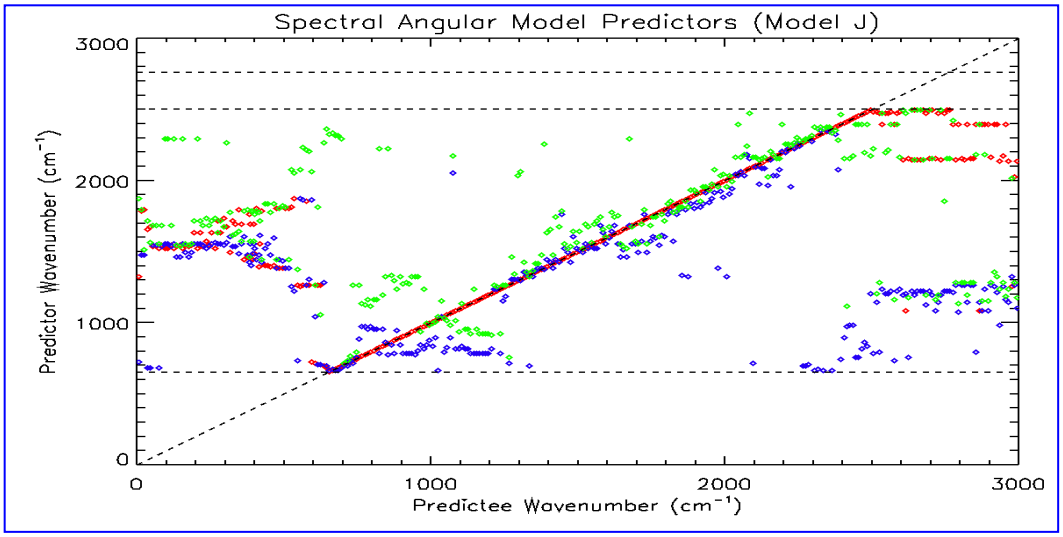

Fig. 2 Selections of predicting radiances (y-axis) for the estimation of spectral fluxes (x-axis) at each 10 cm-1 wavenumber band, with IASI radiance observations in 650-2500 cm-1 range. There are three selected predicting radiances wavenumbers at each spectral band, represented by colors red, blue and green.

.

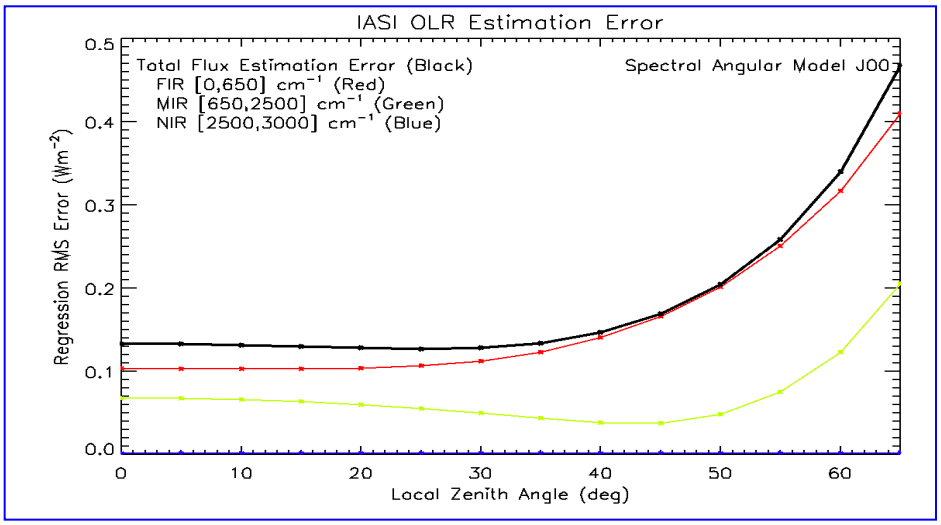

Fig. 3 RMS regression errors for the total OLR estimation, as a function of the observing local zenith angle, range from 0.13 - 0.47 Wm-2, and are dominated by flux estimation errors from the “FIR” spectral domain.

Note that the CrIS OLR algorithm shares the similar estimation principle and model design, except some part of the mid thermal spectrum not directly observed by CrIS would have to be estimated from the observed CrIS radiances.

2.2 Data availability

Table 2 provide the data temporal coverage of operational products of IASI and CrIS observations. **Figure 4** shows the observation local time for the HIRS, IASI and CrIS data onboard of the respective TIROS-N, Metop and JPSS-series satellites.

Table 2 Data availability of IASI and CrIS observations.

Satellite / Instrument	Data Type	Period of Observations
M02/Metop-A IASI	Level 1C	2007-05-21 to 2021-10-15
M01/Metop-B IASI	Level 1C	2013-08-01 to present
M03/Metop-C IASI	Level 1C	2019-07-06 to present
Suomi-NPP CrIS	NSR SDS (prior to 2017-03-08); FSR SDS	2012-04-19 to 2021-05-21 (Degraded since 2021.05.21 without OLR retrievals)
NOAA20/JPSS-01 CrIS	FSR SDS	2017-03-08 to present (with significant missing in 2021.05)
NOAA21/JPSS-02 CrIS	FSR SDS	2023-04-12 to present

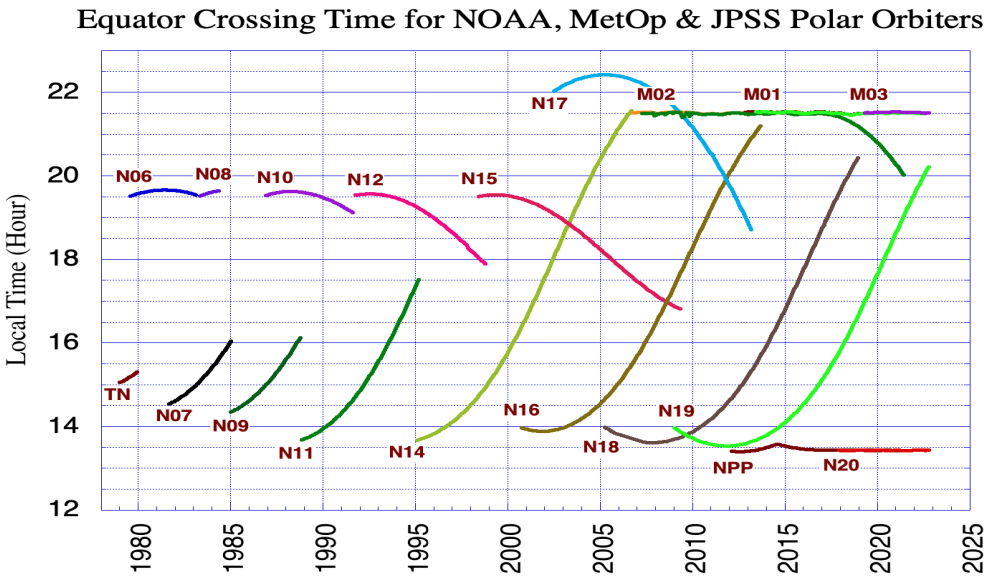

Fig. 4 Equator crossing times for the ascending orbit of the NOAA POES TIROS-N, Metop and JPSS-series satellites.

Inter-satellite Calibration

3.1 Calibrate M02 IASI against M02 HIRS

The intermediate upgrade of the Daily OLR CDR v1.3 is meant to ensure the continued data availability and continuity of the current operational Daily OLR CDR v01r02. The newly added IASI and CrIS OLR retrievals are thus calibrated to the absolute radiometric standard of the v01r02 Daily OLR CDR, that is the HIRS OLR from NOAA-9.

The HIRS OLR and IASI/CrIS regression models are determined with simulated radiation radiances and fluxes databases with similar configurations. However, due to the significant differences in the instruments and the OLR retrieval algorithms, the OLR retrievals are showing some discrepancies. The inter-satellite calibration serves the purpose to eliminated the global and regional differences between the HIRS-retrieved OLR and the IASI/CrIS-retrieved OLR.

The inter-satellite calibration between the M02-HIRS and M02-IASI is the primary tool to maintain the continuity of the OLR CDR.

The method adopted to calibrate M02-IASI to M02-HIRS is the zonal adjustments with linear equations that is dependent on the IASI OLR. We found that the global bias adjustment or theme-dependent bias adjustment are insufficient to produce acceptable agreement between the two retrievals.

The zonal adjustments calibration equations were determined by the data from the respective OLR monthly ascending and descending 2.5° gridded maps, over the common period of 2007.01 – 2016.11. (HIRS data post 2016.12 started to show significant increase of noises.)

For the M02 IASI OLR retrievals within the latitude band φ_i, the adjusted M02 IASI OLR is obtained through the linear adjustment

$$OLR_{M02IASI}^{Adjusted}(\varphi_i) = a_0(\varphi_i) + a_1(\varphi_i)\, OLR_{M02IASI}(\varphi_i) \qquad (6)$$

where φ_i is the 2.5° latitudinal band and a's are the regression coefficients for the corresponding latitudinal band.

Figure 5 shows sample comparisons for the biases between M02 IASI and M02 HIRS, before and after the inter-satellite adjustment, where significant improvements can be seen over the ITCZ and other convective cloud zones.

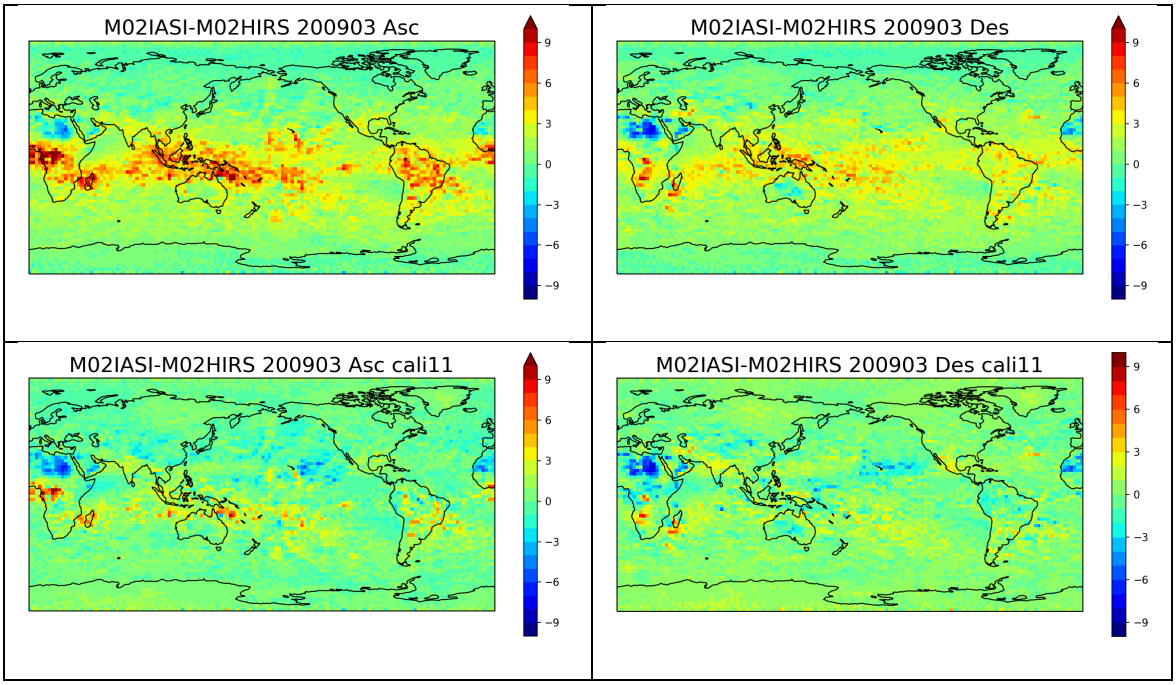

Fig. 5 Monthly mean nodal maps of OLR differences between M02-IASI and M02-HIRS for March 2009 before (top row) and after (bottom row) the application of the zonal intersatellite calibration adjustment.

3.2 Calibrate remaining IASI/CrIS against M02 IASI

For the OLR retrievals from M01, M03 IASI and NPP, J01 and J03 CrIS, they are adjusted by a global bias relative to M02-IASI, determined with the field-of-view (FOV) collocated OLR retrievals over long overlapping time.

Changes from Daily OLR CDR v1.2 to v1.3

The changes in Daily OLR CDR from v1.2 to v1.3 are shown in this section, and the v1.3 is making improvements in most cases. The CERES SYN1deg-Daily Ed4.1 and EBAF Ed4.2 OLR products are used for the performance assessment.

4.1 Evaluation with CERES SYN1deg data

The Daily OLR CDR v1.2 (aka, the current operational product v01r02) and the newly constructed v1.3, with IASI and CrIS OLR are compared to the CERES SYN1deg-Daily Ed4.1 OLR product.

Figure 6 shows the average OLR differences for v1.2 and v1.3 Daily OLR CDR, relative to the CERES SYN1deg-Daily Ed4.1 OLR product, over 2000.03-2022.12 period. The significant reduction of biases in v1.3 can be found in western Pacific, sub-tropics, and over Sahara and Arabian deserts.

Figure 7 shows the standard deviation of the OLR differences for v1.2 and v1.3 Daily OLR CDR, relative to CERES SYN1deg-Daily Ed4.1 OLR product. The reduction of random errors in v1.3 can be found in tropics and sub-tropics, especially over the western Pacific warm pool, and South America regions – attributed to both better temporal sampling provided with the additional IASI and CrIS observations, particularly with the CrIS observations from the afternoon orbits, and higher accuracy of hyperspectral IASI and CrIS OLR retrievals.

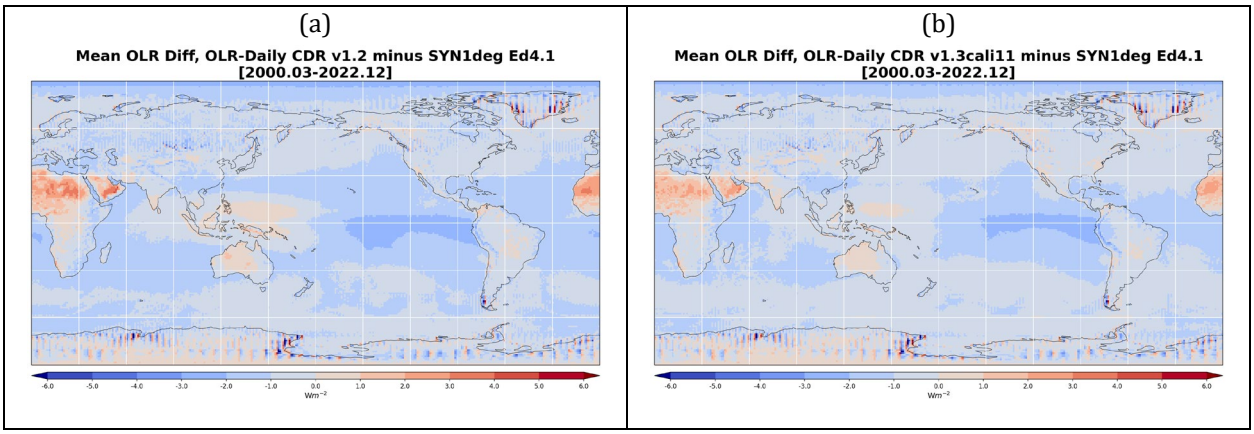

Fig. 6 Mean OLR differences for (a) v1.2 and (b) v1.3 Daily OLR CDR, relative to CERES SYN1deg-Daily Ed4.1 OLR product, over 2000.03-2022.12 period.

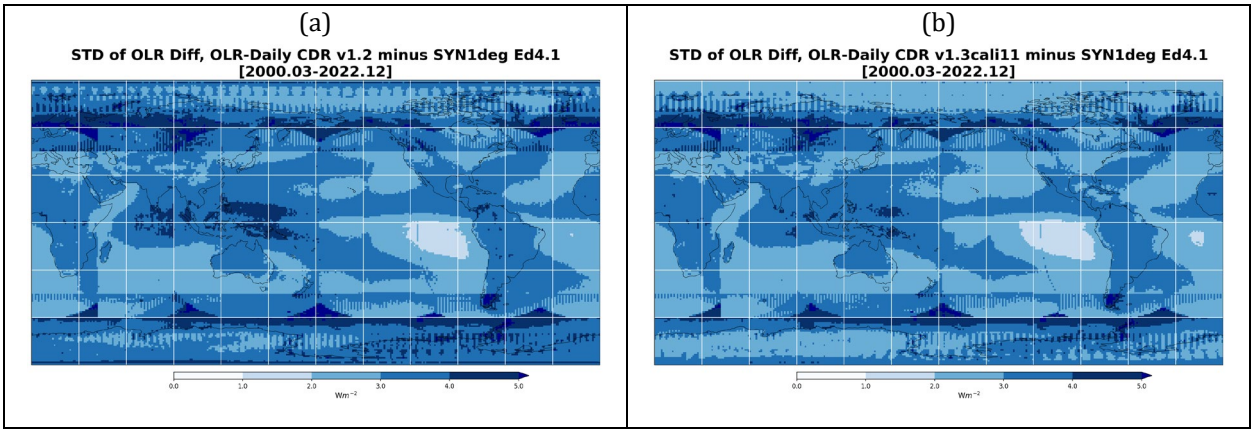

Fig. 7 Standard Deviation of OLR differences for (a) v1.2 and (b) v1.3 Daily OLR CDR, relative to CERES SYN1deg-Daily Ed4.1 OLR product, over 2000.03-2022.12 period.

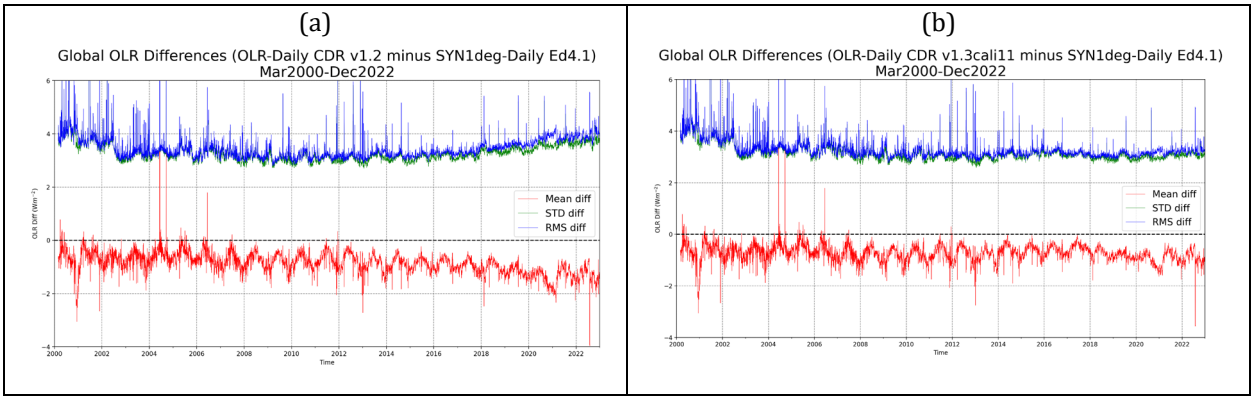

Fig. 8 Global mean OLR differences for (a) v1.2 and (b) v1.3 Daily OLR CDR, relative to CERES SYN1deg-Daily Ed4.1 OLR product, over 2000.03-2022.12 period.

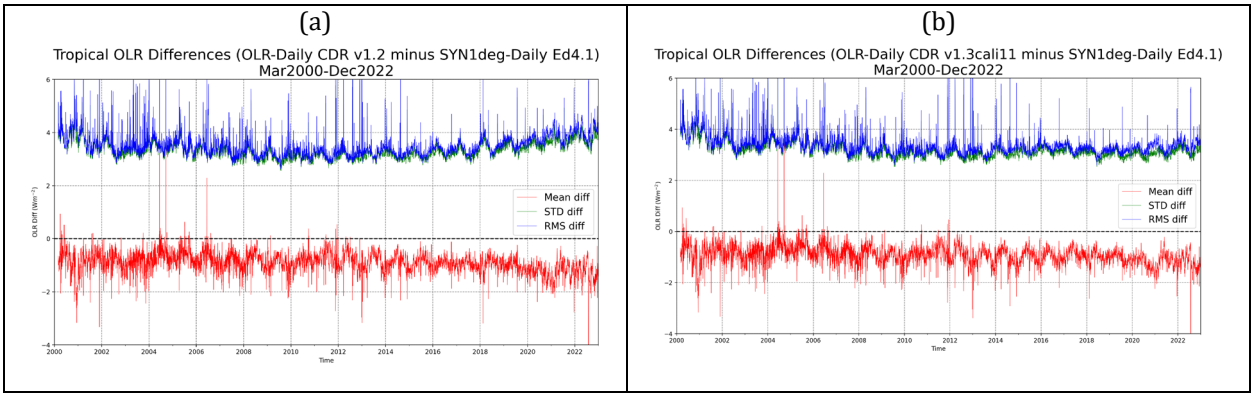

Fig. 9 Tropical 20S-20N mean OLR differences for (a) v1.2 and (b) v1.3 Daily OLR CDR, relative to CERES SYN1deg-Daily Ed4.1 OLR product, over 2000.03-2022.12 period.

Figures 8 and 9 show the time series of the mean, standard deviation, and rms OLR differences for Daily OLR CDR v1.2 and v1.3, relative to the CERES SYN1deg-Daily Ed4.1 product, for global and tropical domain average, respectively. The notable changes are in the mean and standard deviation of the OLR differences where the gradual increases of the OLR differences (negatively) between v1.2 and SYN1deg after 2016 have been removed in v1.3. This is likely be attributed to the added diurnal sampling time with the IASI and CrIS observations. The increased standard deviation in v1.2 after 2016 has been brought down to level in the v1.3, thanks to the better OLR retrievals from IASI and CrIS and the removal of some bad/noisy HIRS OLR retrievals through QC.

Figures 10 and 11 show the time series of the mean differences of the OLR anomalies for Daily OLR CDR v1.2 and v1.3, relative to the CERES SYN1deg-Daily Ed4.1 product, for global and tropical domains, respectively. Similarly, the negative departures of the OLR anomalies in v1.2 vs SYN1deg after 2016 no longer present in the v1.3.

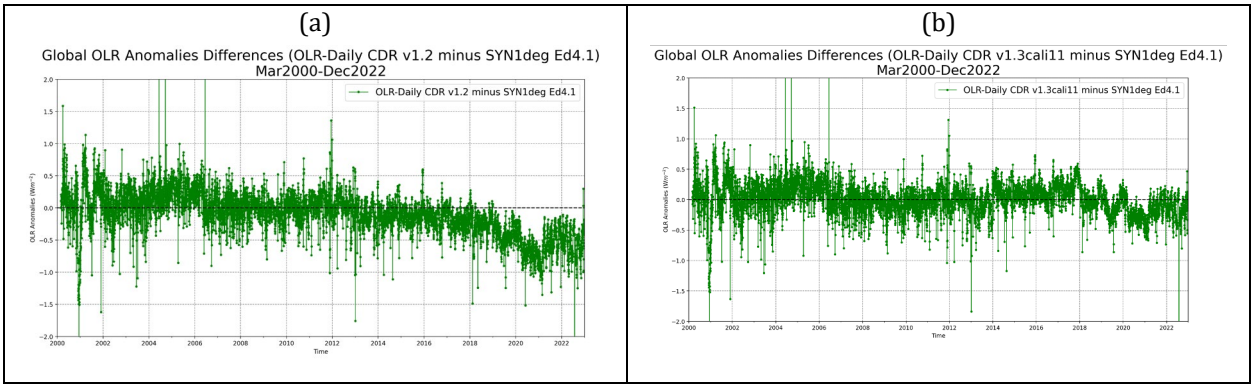

Fig. 10 Differences of global OLR anomalies for (a) v1.2 and (b) v1.3 Daily OLR CDR, relative to CERES SYN1deg-Daily Ed4.1 OLR product, over 2000.03-2022.12 period.

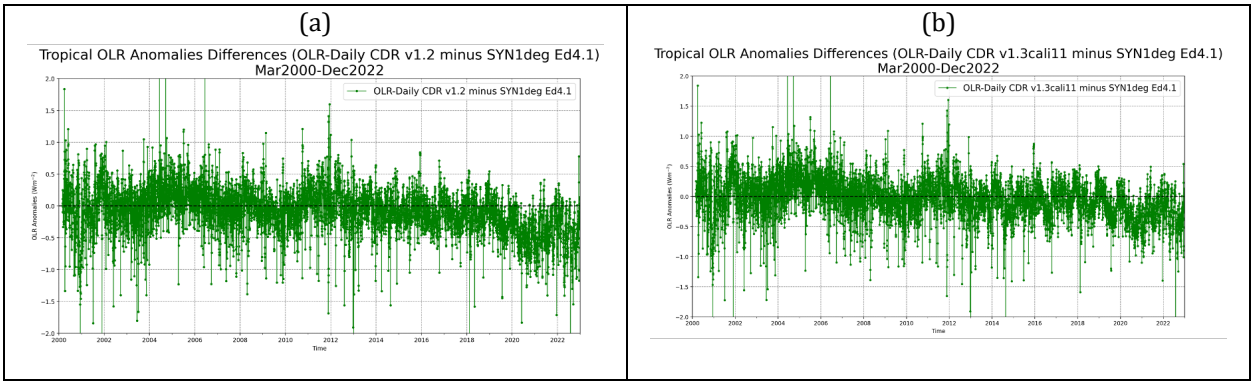

Fig. 11 Differences of tropical OLR anomalies for (a) v1.2 and (b) v1.3 Daily OLR CDR, relative to CERES SYN1deg-Daily Ed4.1 OLR product, over 2000.03-2022.12 period.

Figures 12 shows the changes in the global mean and standard deviation of OLR differences for various pairs, to demonstrate the positive impact of the addition of IASI and CrIS in the Daily OLR CDR production. Better stability in both the mean and standard deviation of the OLR differences relative to SYN1deg product is shown in the v1.3 product.

Figures 13 compares the standard deviation of OLR differences, relative to SYN1deg data, as a function of latitude, averaged over 2000.03-2022.12. Clear improvement is made in the v1.3 product across all the latitudinal zones, with greater improvement in the higher latitude zones.

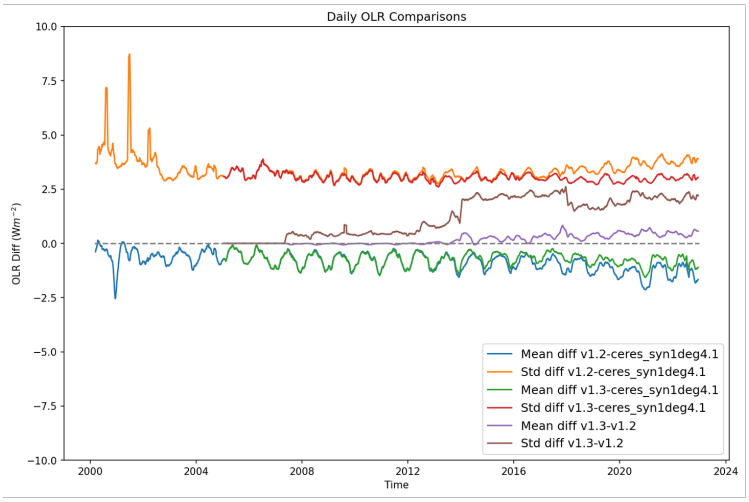

Fig. 12 Global mean OLR differences for v1.2 and v1.3 Daily OLR CDR, relative to CERES SYN1deg-Daily Ed4.1 OLR product. It shows improved stability (see green curve) and reduced random errors (red curve) in v1.3 Daily OLR CDR, particularly after 2014.

Fig. 13 Comparison of the standard deviation of zonal OLR differences v1.2 (blue) and v1.3 (orange) Daily OLR CDR, relative to CERES SYN1deg-Daily Ed4.1 OLR product. It shows significant reduction of the uncertainties across the latitudinal zones.

Table 3 summarize the statistics of the Daily OLR CDR performances, in reference to the CERES SYN1deg-Daily Ed4.1 product. The most significant changes are in the trend in the anomaly differences. The global anomalies differences in Daily OLR CDR v1.2 has a -0.323±0.009 Wm-2/decade trend, relative to SYN1deg-1deg, while it is greatly improved to **-0.091±0.009 Wm-2/decade for v1.3.**

Table 3 summarize the statistics of the Daily OLR CDR performances, in reference to the CERES SYN1deg-Daily Ed4.1 product. The most significant changes are in the trend in the anomaly differences. The global anomalies in Daily OLR CDR v1.2 has a -0.323±0.009 Wm-2/decade trend, relative to SYN1deg-1deg Ed4.1, while this is greatly improved to **-0.091±0.009 Wm-2/decade for v1.3.**

Table 3 Summary statistics for the evaluation of Daily OLR CDR v1.2 and v1.3, in reference to CERES SYN1deg-daily Ed4.1 product, over 2000.03-2022.12 period.

	CDRv1.2 – SYN1deg4.1	CDRv1.3 – SYN1deg4.1
Global Mean diff	-0.86	**-0.73**
Global Std diff	3.33	**3.20**
Global RMS diff	3.46	**3.30**
Tropical Mean diff	-0.89	-0.92
Tropical Std diff	3.37	3.21
Tropical RMS diff	3.50	3.37
Slope of global Anom diff	-0.323 ± 0.009	**-0.091 ± 0.009**
Slope of tropical Anom diff	-0.196 ± 0.012	**-0.181 ± 0.012**
Corr of Global Anom	0.933	0.958
Corr of Tropical Anom	0.981	0.982

4.2 Evaluation with CERES EBAF data

The monthly integrated Daily OLR CDR v1.2 and v1.3 products are compared to CERES EBAF Ed4.2 product.

Figure 14 shows the average OLR differences for v1.2 and v1.3 Daily OLR CDR, relative to the CERES EBAF Ed4.2 OLR product, over 2000.03-2022.12 period. The reduction of biases in v1.3 can be found in sub-tropics and Sahara and Arabian deserts.

Figure 15 shows the standard deviation of the OLR differences for v1.2 and v1.3 Daily OLR CDR, relative to CERES EBAF Ed4.2 OLR product. The reduction of random errors in v1.3 can be found in tropics, sub-tropics, and northern Pacific.

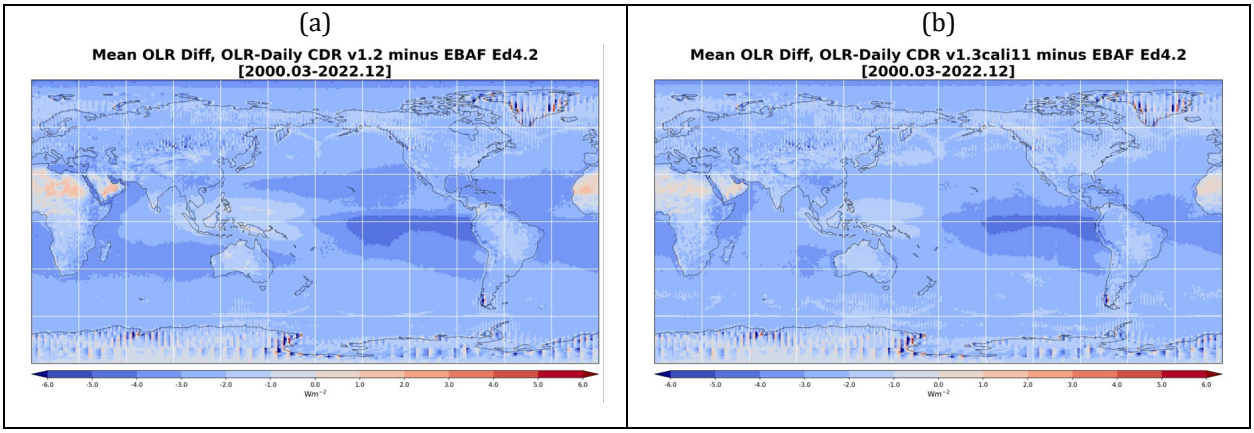

Fig. 14 Mean OLR differences for (a) v1.2 and (b) v1.3 Daily OLR CDR, relative to CERES EBAF Ed4.2 OLR product, over 2000.03-2022.12 period.

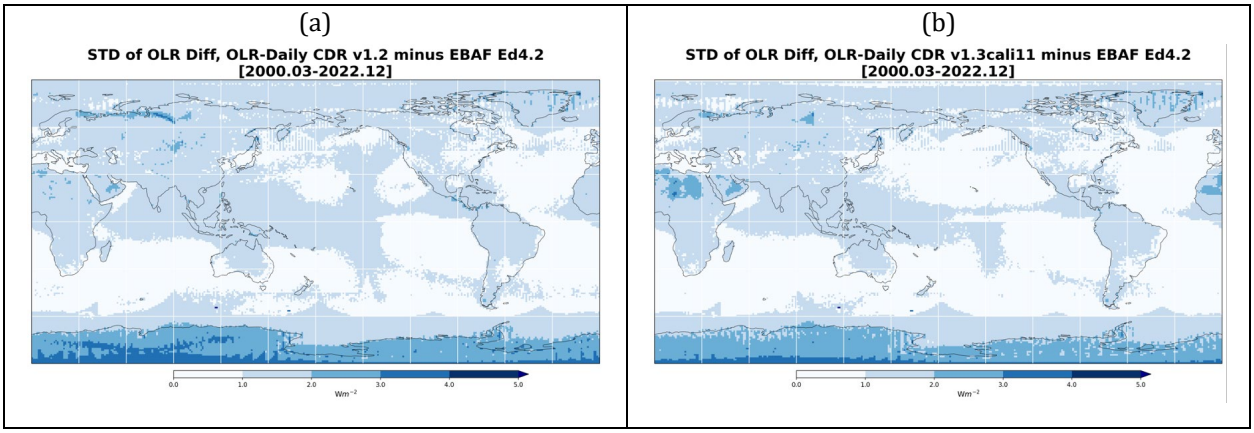

Fig. 15 Standard Deviation of OLR differences for (a) v1.2 and (b) v1.3 Daily OLR CDR, relative to CERES EBAF Ed4.2 OLR product, over 2000.03-2022.12 period.

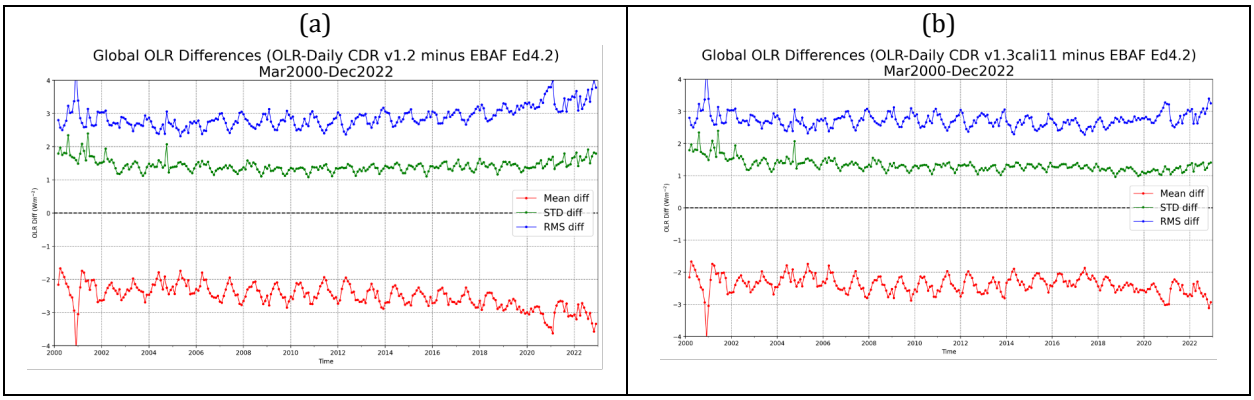

Fig. 16 Global mean OLR differences for (a) v1.2 and (b) v1.3 Daily OLR CDR, relative to CERES EBAF Ed4.2 OLR product, over 2000.03-2022.12 period.

Figures 16 shows the time series of the mean, standard deviation, and rms OLR differences for Daily OLR CDR v1.2 and v1.3, relative to the CERES SYN1deg-Daily Ed4.1 product, for global domain average. Similar to the comparison to SYN1deg, the gradual increases of the OLR differences (negatively) between v1.2 and EBAF after 2016 have been removed in v1.3.

Figures 17 and 18 show the time series of the OLR anomalies from Daily OLR CDR v1.2 and v1.3, and the CERES EBAF Ed4.2 product, for global and tropical domains, respectively. The Daily OLR CDR v1.3 OLR anomalies track accurately with those from the EBAF Ed4.2 product, eliminating the apparent departures in v1.2 after 2018.

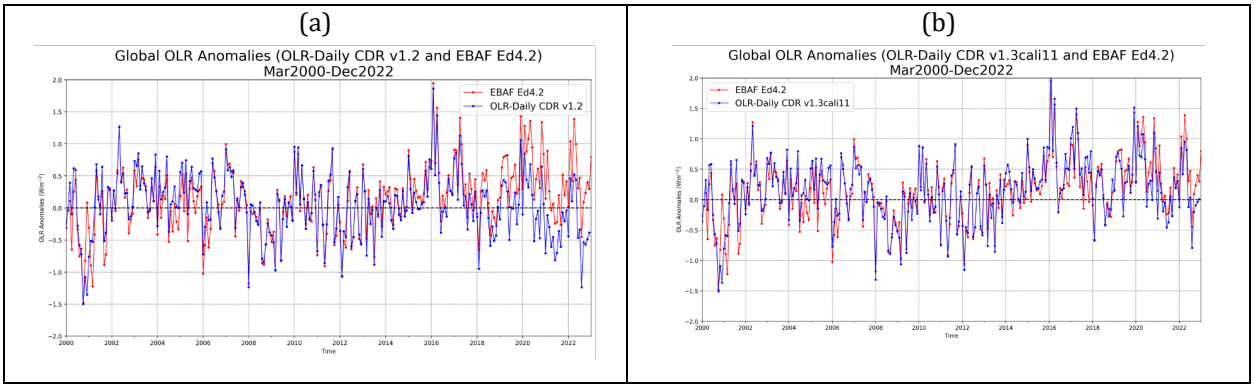

Fig. 17 Differences of global OLR anomalies for (a) v1.2 and (b) v1.3 Daily OLR CDR, relative to CERES EBAF Ed4.2 OLR product, over 2000.03-2022.12 period.

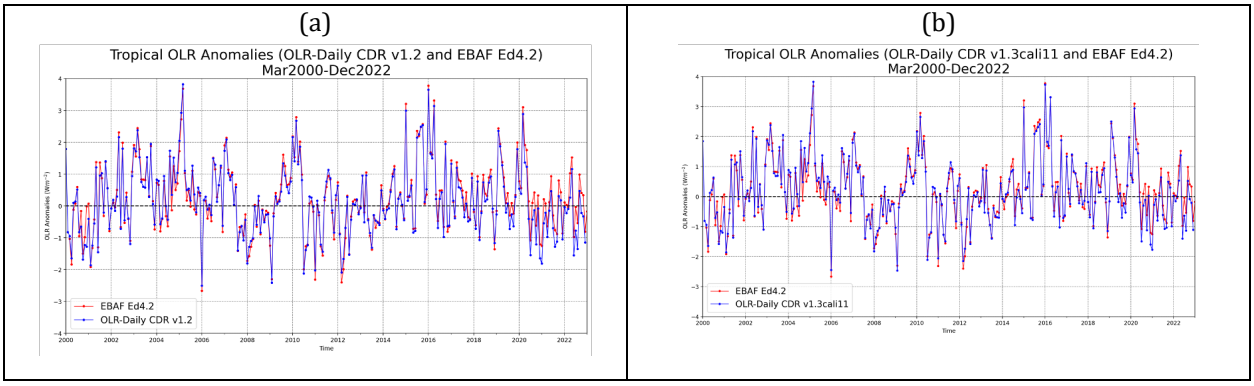

Fig. 18 Differences of tropical OLR anomalies for (a) v1.2 and (b) v1.3 Daily OLR CDR, relative to CERES EBAF Ed4.2 OLR product, over 2000.03-2022.12 period.

Figures 19 and 20 show the time series of the mean differences of the OLR anomalies for Daily OLR CDR v1.2 and v1.3, relative to the CERES EBAF Ed4.2 product, for global and tropical domains, respectively. The spurious trends of the in OLR anomaly differences in v1.2 post 2016 are eliminated in v1.3.

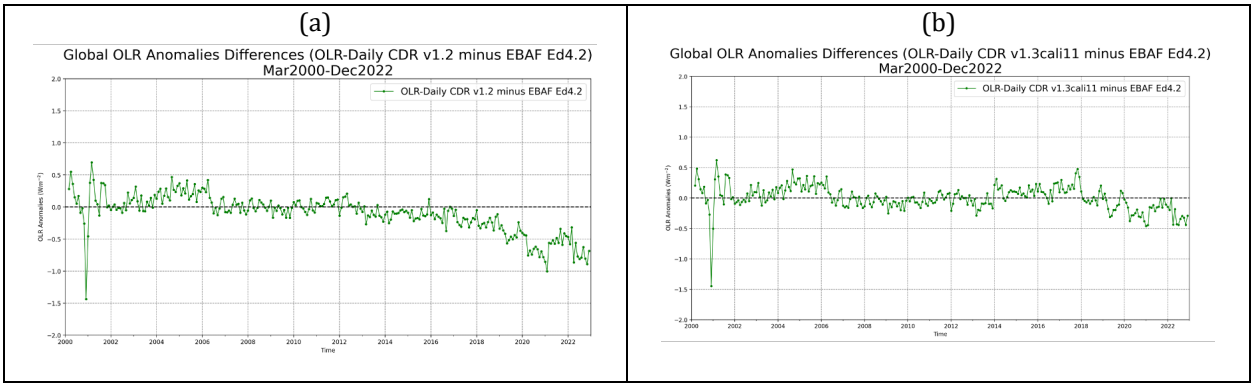

Fig. 19 Differences of global OLR anomalies for (a) v1.2 and (b) v1.3 Daily OLR CDR, relative to CERES SYN1deg-Daily Ed4.1 OLR product, over 2000.03-2022.12 period.

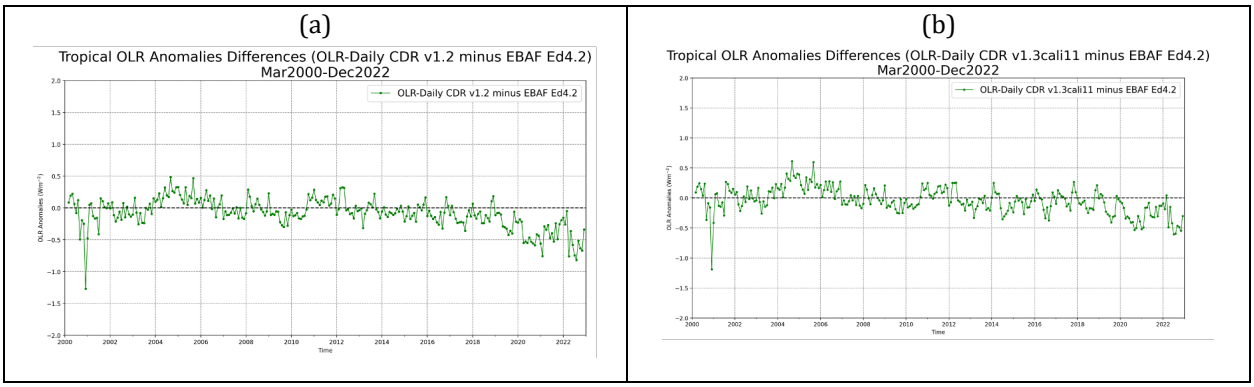

Fig. 20 Differences of tropical OLR anomalies for (a) v1.2 and (b) v1.3 Daily OLR CDR, relative to CERES SYN1deg-Daily Ed4.1 OLR product, over 2000.03-2022.12 period.

.

Table 4 summarize the statistics of the Daily OLR CDR performances, in reference to the CERES EBAF Ed4.2 product. The most significant changes are in the trend in the anomaly differences. The global anomalies in Daily OLR CDR v1.2 has a -0.329±0.037 Wm-2/decade trend, relative to EBAF Ed4.2, while this is greatly improved to **-0.097±0.036 Wm-2/decade for v1.3.**

Table 4 Summary statistics for the evaluation of Daily OLR CDR v1.2 and v1.3, in reference to CERES EBAF Ed4.2 product, over 2000.03-2022.12 period.

	CDRv1.2 – EBAF4.2	CDRv1.3 – EBAF4.2
Global mean diff	-2.51	-2.38
Global Std diff	1.44	1.34
Global rms diff	2.90	2.74
slope of Global Anom diff	-0.329 ± 0.037	**-0.097 ± 0.036**
slope of Tropical Anom diff	-0.169 ± 0.038	**-0.154 ± 0.036**

References

Lee, H.-T., 2014: Outgoing Longwave Radiation – Daily Climate Data Record Algorithm Theoretical Basis Document. CDRP-ATBD-0526 Rev 1. NCDC Climate Data Record Program

Schreck, C. J., H.-T. Lee and K. Knapp, 2018: HIRS Outgoing Longwave Radiation—Daily Climate Data Record: Application toward Identifying Tropical Subseasonal Variability. Remote Sens. 2018, 10, 1325; https://doi.org/10.3390/rs10091325

Lee, H.-T., R. G. Ellingson, and A. Gruber, 2010: Development of IASI outgoing longwave radiation algorithm. Proceedings of the 2nd IASI International Conference, Annecy, France, January 25-29, 2010.

Turner, E. C., H.-T. Lee and S. F. B. Tett, 2015: Using IASI to simulate the total spectrum of outgoing long-wave radiances, Atmos. Chem. Phys., 15, 6561-6575, doi:10.5194/acp-15-6561-2015.

IASI Level 1 Product Guide: PDF_IASI_LEVEL_1_PROD_GUIDE.pdf, EUM.EPS.SYS.SPE.990003 v9e. Dec 3, 2014.

IASI Level 1 Product Format Specification, 2011: PDF_IASI_LEVEL_1_PFS product format spec. Dec 14, 2011.

Data Quality Summary for CERES EBAF Ed4.1: CERES_EBAF_Ed4.1_DQS.pdf v.3 released 12/9/2021

Data Quality Summary for CERES EBAF Ed4.2: CERES_EBAF_Ed4.2_DQS.pdf v.0 released 12/9/2022

Data Quality Summary for CERES SYN1deg-Daily Ed4.1: CERES_SYN1deg_Ed4A_DQS.pdf 4/8/2021

References for CERES products: https://ceres.larc.nasa.gov/data/documentation/#ssf

Acknowledgment

This work is funded by the NOAA NCEI CDR program.

The IASI Level 1c data are obtained through NOAA CLASS data service.

The CrIS SDS data obtained through NESDIS STAR/UMD ESSIC data service.

These CERES EBAF and SYN1deg data were obtained from the NASA Langley Research Center CERES ordering tool at https://ceres.larc.nasa.gov/data/.

The IASI Level 1c data reader software is modified from Eumetsat software “Generic EPS-Tools: EPS format Interactive Data Language (IDL) readers”, EPS_OO_IDL_V1_6_RELEASE.